Volume 17 | Number 40 | 28 October 2015 | Pages 26485–27226

PCCP

Physical Chemistry Chemical Physics
www.rsc.org/pccp

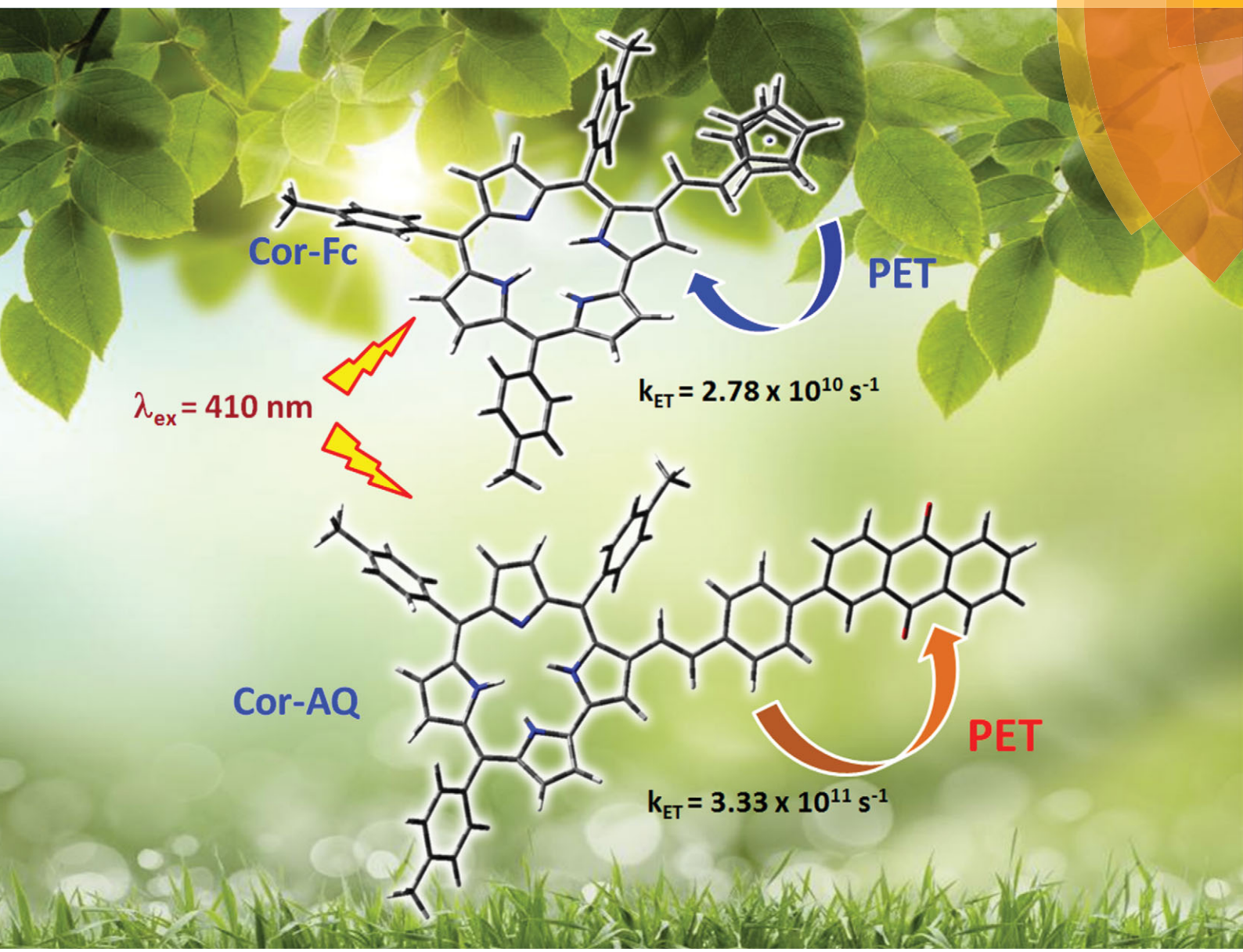

ISSN 1463-9076

ROYAL SOCIETY OF CHEMISTRY

PAPER
Prakriti R. Bangal, Lingamallu Giribabu *et al.*
Corrole–ferrocene and corrole–anthraquinone dyads: synthesis, spectroscopy and photochemistry

PCCP

PAPER

View Article Online
View Journal | View Issue

CrossMark click for updates

Cite this: *Phys. Chem. Chem. Phys.*, 2015, **17**, 26607

Corrole–ferrocene and corrole–anthraquinone dyads: synthesis, spectroscopy and photochemistry†

Jaipal Kandhadi,[a] Venkatesh Yeduru,[ab] Prakriti R. Bangal*[ab] and Lingamallu Giribabu*[ab]

Received 2nd May 2015,
Accepted 24th July 2015

DOI: 10.1039/c5cp02565f

www.rsc.org/pccp

Two different donor–acceptor systems based on corrole–ferrocene and corrole–anthraquinone having the '*Olefin Bridge*' at the β-pyrrole position have been designed and synthesized. Both the dyads corrole–ferrocene (**Cor–Fc**) and corrole–anthraquinone (**Cor–AQ**) are characterized by elemental analysis, ESI-MS, ^{1}H NMR, UV-Visible, fluorescence spectroscopies (steady-state, femtosecond time-resolved), femtosecond transient absorption spectroscopy (fs-TA) and electrochemical methods. ^{1}H-NMR shows that two doublets at 6.50 and 7.25(δ) ppm belong to vinylic protons, which are characteristic of the formation of dyads. UV-Visible absorption spectra showed that dyads are merely superpositions of their respective constituent monomers and dominated by corrole $S_1 \leftarrow S_0$ (Q-band) and $S_2 \leftarrow S_0$ (Soret band) transitions with a systematic red-shift of both Soret and Q-bands along with the broadening of the bands. A prominent splitting of the Soret band for both the dyads is observed due to bulky substitutions at the peripheral position, which deviate from the planarity of the corrole macrocycle. Both the dyads exhibit significant fluorescence emission quenching (95–97%) of corrole emission compared to the free-base corrole monomer. Emission quenching is attributed to the excited-state intramolecular photoinduced electron transfer (PET) from corrole to anthraquinone in the **Cor–AQ** dyad, whereas in the **Cor–Fc** dyad it is reversed. The electron-transfer rates (k_{ET}) for **Cor–AQ** and **Cor–Fc** were found to be 3.33×10^{11} and 2.78×10^{10} s^{-1}, respectively. Despite their very different driving forces, charge separation (CS) and charge recombination (CR) are found to be in identical timescales.

Published on 31 luglio 2015. Downloaded by Fail Open on 23/07/2025 10:08:23.

Introduction

Over the past few years, considerable efforts have been devoted to the design, synthesis and scrutiny of donor–acceptor (D–A) systems for efficient intramolecular photoinduced electron transfer (PET) or excitation energy transfer (EET), thus mimicking the reaction centre of natural photosynthetic organisms.[1–8] Among various systems, porphyrins are of particular importance as building blocks for the construction of models.[9–11] Porphyrins almost dominate the study of D–A systems, due to their easy availability and large body of information on their synthetic strategies and photophysical processes.[12–15] In spite of this many other porphyrinoids have interesting photophysical properties and have been used as photoactive components in the construction of models mimicking various stages of photosynthesis. For example phthalocyanines,[16,17] subphthalocyanines,[18] chlorins,[19] fused porphyrins,[20] core modified porphyrins,[21] expanded porphyrins,[22] contracted porphyrins,[23] N-confused porphyrins,[24] and BODIPY[25] or corroles[26] have been successfully used for making D–A systems. Of these, we are particularly interested in corrole based D–A systems.

The corrole macrocycle is a contracted analogue of a porphyrin in which one *meso* position has been eliminated, resulting in a direct pyrrole–pyrrole bond, yet possessing the 18-π electron aromaticity of porphyrins.[27] When compared with porphyrins, corroles are tribasic aromatic macrocycles exhibiting interesting properties which include stabilization of unusual high oxidation states of transition metal centres, lower oxidation potentials, higher fluorescence quantum yields, larger Stokes shift, and relatively high extinction coefficients in the red part of the optical spectrum.[28–30] A few D–A systems based on corroles have been reported in the literature to understand natural photosynthetic phenomena.[31–37] These D–A systems have been constructed either at the *meso*-phenyl position or at the axial position of resident metal ion of the corrole macrocycle. For example, our group has utilized the axial position/s of the resident metal ion of the corrole macrocycle, constructed hetero oligomers and studied the effect of metal ion on PET and EET reactions.[31,32] Ngo *et al.* have constructed mixed corrole–porphyrin multichromophoric systems by using *meso* positions of the macrocycle and studied the singlet–singlet energy

[a] *Inorganic & Physical Chemistry Division, CSIR-Indian Institute of Chemical Technology, Habsiguda Hyderabad-500007, Telangana, India. E-mail: giribabu@iict.res.in; Fax: +91-40-27160921; Tel: +91-40-27191724*
[b] *Academy of Scientific and Innovative Research (AcSIR), New Delhi, India*

† Electronic supplementary information (ESI) available: ^{1}H NMR and ESI-MS spectra, cyclic voltammograms, fluorescence spectra, optimized structures, frontier molecular orbitals, and transient absorption spectra. See DOI: 10.1039/c5cp02565f

Published on 31 luglio 2015. Downloaded by Fail Open on 23/07/2025 10:08:23.

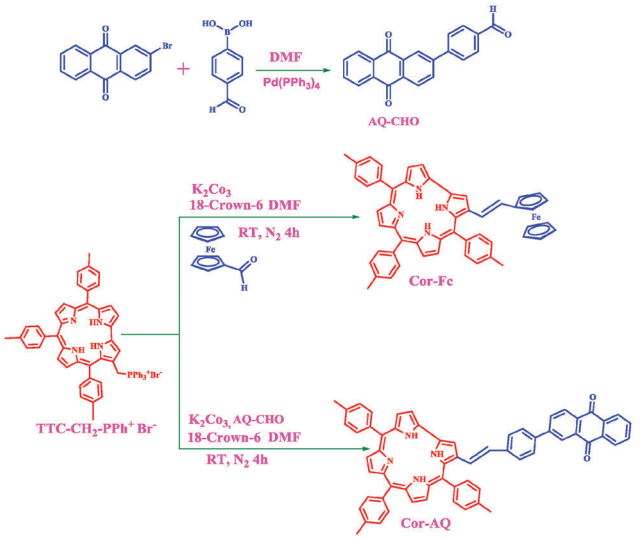

Fig. 1 Synthetic scheme of **Cor–Fc** and **Cor–AQ** dyads.

transfer process by using transient absorption spectroscopy.[34] D'Souza and co-workers have used *meso* positions of donor corrole and constructed corrole–fullerene dyads at a rate of charge separated state $\sim 10^{10}$–10^{11} s^{-1}.[34] Recently, we have utilized the β-pyrrole position of corrole macrocycle and constructed corrole–polycyclic aromatic hydrocarbon (either pyrene or fluorene) dyads.[38] The excited state properties revealed that there is an energy transfer from polycyclic aromatic hydrocarbon to the corrole macrocycle. During the course of our research in the construction of D–A systems by using β-pyrrole position of the corrole macrocycle, here we reported the synthesis, characterization and photophysical properties of corrole–anthraquinone, (**Cor–AQ**) and corrole–ferrocene, (**Cor–Fc**) conjugates (Fig. 1). Ferrocene is a stable aromatic sandwich organometallic compound and numerous porphyrin–ferrocene conjugates have been reported in the literature, in which a photoinduced electron transfer takes place from ferrocene to the excited state of porphyrin.[39,40] In contrast, quinone is an ultimate electron acceptor during natural photosynthesis resulting in a long-lived, charge-separated state and a substantial number of porphyrin–quinone systems has been reported in the literature for mimicking photosynthesis.[9] Both the dyad systems (**Cor–AQ** & **Cor–Fc**) have been completely characterized by elemental analyses, MALDI-MS, UV-Visible, ^{1}H NMR and fluorescence (steady-state and time-resolved) spectroscopies as well as electrochemical methods. In addition, we compared the photophysical properties of corrole–ferrocene and corrole–anthraquinone dyads for the first time to the best of our knowledge.

Experimental section

Materials

Commercially available reagents and chemicals were used in the present investigations. Analytical reagent grade solvents were used for synthesis, and distilled laboratory grade solvents were used for column chromatography. Dry chloroform and dichloromethane were prepared by argon-degassed solvent through activated alumina columns. Nitrogen gas (oxygen-free) was passed through a KOH drying column to remove moisture. Neutral Alumina (mesh 60–325, Brockmann activity1) was used for column purification. All the reactions were carried out under a nitrogen or argon atmosphere using dry degassed solvents and the apparatus was shielded from ambient light.

Synthesis

5,10,15-tri tolyl corrole (**TTC**) and corrole phosphonium salt (TTC-CH_2-$PPh_3^+Br^-$) were synthesized according to the reported procedures.[38,41]

Synthesis of the corrole–ferrocene dyad (Cor–Fc). Ferrocene-2-carboxaldehyde (12 mg, 0.055 mmol), 18-crown-6 (10 mg, 0.04 mmol), anhydrous potassium carbonate (15 mg, 0.1 mmol) and corrole phosphonium salt TTC-CH_2-PPh_3 + Br^- (50 mg, 0.055 mmol) were dissolved in 6 ml of dry DMF. The reaction mixture was stirred at room temperature for 4 h under a nitrogen atmosphere. Solvent was removed under reduced pressure, washed with water, and dried under vacuum. The obtained solid material was subjected to silica gel column chromatography and eluted with the $CHCl_3$: hexane (50 : 50 v/v) mixture. The solvent front running brown color band was collected and recrystallized from $CHCl_3$: hexane to get the desired product in 65% yield. Anal. calcd for $C_{52}H_{42}FeN_4$ % (778.70): C, 80.20; H, 5.44; N, 7.19. Found C, 80.25; H, 5.40; N, 7.25. ESI-MS: m/z = 780 (M^+ + 2H). ^{1}H-NMR (500 MH_Z, $CDCl_3$, TMS) δ (PPM): −2.85 (s, 3H), 2.66 (s, 6H), 2.77 (s, 3H), 4.16 (s, 5H), 4.26 (d, 4H), 6.78 (d, 1H), 7.49–7.7 (m, 7H), 7.97–8.23 (m, 12H), 8.92 (d, 1H).

Synthesis of 4-(9,10-dihydro-9,10-dioxoanthracen-6-yl)benzaldehyde (AQ-CHO). This compound was synthesized by slightly modifying the literature procedure.[42] 2-Bromoanthracene-9,10-dione (50 mg, 0.174 mmol) and (4-formylphenyl)boronic acid (30 mg, 0.209 mmol) were dissolved in 12 ml of dry DMF. To this 3 ml of 2 M Na_2CO_3 solution was added and the reaction mixture was degassed for 30 min. $Pd(PPh_3)_4$ (5 mg, 0.0174 mmol) was added to a reaction mixture and refluxed for 18 h under nitrogen atmosphere. The reaction was monitored through TLC. After completion of the reaction, the compound was extracted with dichloromethane, organic layer was separated, dried and the residue was purified by column chromatography using silica gel with an eluent of ethylacetate : hexane (2 : 8, v/v) to get the desired compound as a yellow solid (yield, 70%). Anal. calcd for $C_{21}H_{12}O_3$ % (312.3): C, 80.76; H, 3.87; N, 15.37. Found C, 80.75; H, 3.90; N, 15.35. ESI-MS: m/z = 311 (M^+ + H). ^{1}H-NMR (500 MH_Z, $CDCl_3$, TMS) δ (PPM): 7.83–7.93 (dd, 4H), 8.09 (dd, 3H), 8.34–8.45 (dd, 3H), 8.59 (s, 1H), 10.1 (s, 1H).

Synthesis of corrole–anthraquinone dyad (Cor–AQ). We have adopted a similar procedure for the synthesis of **Cor–Fer** from this compound. The only difference is that, we have used 4-(9,10-dihydro-9,10-dioxoanthracen-6-yl)benzaldehyde instead of ferrocene-2-carboxaldehyde. (yield, 75%). Anal. calcd for $C_{62}H_{46}N_4O_2$ % (877): C, 84.91; H, 5.06; N, 6.39. Found C, 84.95; H, 5.00; N, 6.35. ESI-MS: m/z = 877 (M^+ + H). ^{1}H-NMR (500 MH_Z, $CDCl_3$, TMS) δ (PPM): −2.88 (s, 3H), 2.67 (s, 6H), 2.79 (s, 3H), 7.34 (dd, 1H), 7.41–7.75 (m, 12H), 7.96–8.84 (m, 20H), 8.93 (s, 1H).

This journal is © the Owner Societies 2015

Published on 31 luglio 2015. Downloaded by Fail Open on 23/07/2025 10:08:23.

Methods and instrumentation

^{1}H NMR spectra were recorded on a 500 MHz INOVA spectrometer. Cyclic and differential-pulse voltammetric measurements were performed on a PC-controlled electrochemical analyzer (CH instruments model CHI620C). All these experiments were performed with 1 mM concentration of compounds in dichloromethane at a scan rate of 100 mV s^{-1} in which tetrabutyl ammonium perchlorate (TBAP) is used as a supporting electrolyte as documented in our previous reports.[43] The optical thin layer electrochemical studies were carried out with Maya 2000 Ocean Optics software using DT-MINI-2-GS, UV-VIS-NIR LIGHTSOURCE.

Theoretical calculations

Full geometry optimization computations of the **Cor–Fc** and **Cor–AQ** dyads were carried out with the DFT-B3LYP method using the 6-31G* basis set and frequency analysis confirmed that the obtained geometries should be genuine global minimum structures. All calculations were performed with the Gaussian G03 (d01) package on a personal computer.[44]

Steady state absorption and fluorescence measurements

The optical absorption spectra were recorded on a Shimadzu (Model UV-3600) spectrophotometer. Concentrations of solutions are *ca.* 1×10^{-6} M (corrole Soret band) and 5×10^{-5} M (corrole Q-bands). Steady-state fluorescence spectra were recorded on a Fluorolog-3 spectrofluorometer (Spex model, Jobin Yvon) for solutions with optical density at a wavelength of excitation (λ_{ex}) $\approx$0.05. Fluorescence quantum yields (ϕ) were estimated by integrating the fluorescence bands and by using 5,10,15-triphenyl corrole (ϕ = 0.21 in toluene) as the reference compound.[29]

Fluorescence up-conversion/fluorescence optical gate

A detailed description of our femtosecond laser apparatus was described elsewhere.[45] However, in brief, for fluorescence up-conversion study FOG 100-DX system (CDP System Corp. Moscow, Russian Federation) was used. Fundamental laser output ($\sim$500 mW at 800 nm) of the Ti:sapphire oscillator (Mai Tai HP, Spectra Physics) was steered into a CDP2015 frequency conversion unit forming the second harmonic (SH). A beam splitter (BS) is used to split the input beam (SH of fundamental) to excitation and gate (fundamental residual pulses) beams. The excitation beam was directed to a rotating sample cell with the help of six mirrors and one BS. A lens (f = 40 mm) was used to focus excitation beam into the sample. A neutral density (ND) filter was used for the excitation attenuation. The gate beam was directed by two mirrors to a gold-coated retro-reflector mirror connected to 8 ns optical delay line before being focused together with the fluorescence (collected by an achromatic doublet, f = 80 mm) on 0.5 mm type-I BBO crystal. The angle of the crystal was adjusted to phase matching conditions at the fluorescence wavelength of interest. The up-converted signal (in the UV range) was focused with a lens (f = 60 nm) to an input slit of the monochromator (CDP2022D). The intensity of the up-converted radiation was measured using a photomultiplier tube operating in the photon counting mode. Proper filters were used before the detector to eliminate parasitic light from the up-converted signal if any. The polarization of the excitation pulses was set at magic angle relative to that of the gate pulses using Berek's variable wave plate. The sample solutions were placed in a 0.6 mm or 1 mm rotating cell and absorbance of about $\sim$0.6 at excitation wavelength was generally used (yielding a concentration of around 100–200 μM). The FWHM of the instrument response function (IRF) in this setup was calculated to be 240 fs in the 0.4 mm cell and 280 fs in the 1 mm cell. Hence, a time resolution of $<$200 fs could be achieved. For data analysis, the fluorescence time profile at a given emission wavelength $I(\lambda,t)$ was reproduced by the convolution of a Gaussian IRF with a sum of exponential trial function representing the pure sample dynamics $S(t)$. A Gaussian term was added to account for fast non-exponential processes if any owing to vibrational or other solvent relaxation process.

Femtosecond transient absorption/pump–probe

Transient absorption studies were performed using a pump–probe set up of CDP Systems Corporation, ExciPro. The output of optical parametric amplifier (TOPAS prime) was used as pump sources at required wavelength and feed into a spectrometer through a synchronized chopper for 1 kHz repetition rate. A lens (f = 200 mm) was used to adjust the pump diameter while an iris and neutral density filter combination were used to adjust the pump energy. A Berek's variable wave plate was placed in the pump beam and polarization was fixed at the magic angle with respect to the probe pulse. A part of the output of the Ti:sapphire regenerative amplifier (Spitfire Ace, Spectra Physics) with 1 kHz repetition rate and $\sim$100 mW average power at 800 nm was fed to the spectrometer. The power of the 800 nm was reduced to 20–25 mW and focused onto a thin rotating (2 mm) CaF_2 crystal window to generate a white-light continuum. A fraction of this beam was sent to a photodetector which controls speed and phase of the chopper rotation. The beam of white light was collimated with a parabolic mirror (f = 50 mm, 9°). Then this white light was reflected from a beam splitter and mirror into two identical probes and reference beams. Two concave mirrors (f = 150 mm) were used to focus both probe and reference beams to the rotating sample cell. Two lenses (f = 60 mm) created probe and reference images at the entrance surfaces of two optical fibers which are connected to the entrance slit of the imaging spectrometer (CDP2022i). This spectrometer consists of UV-Vis photodiode (Si linear photodiode) arrays and IR Photodiode (GaAS linear photodiode) arrays with spectral response range 200–1000 nm and 900–1700 nm respectively. Quartz cells of 1 mm sample path length were used for all studies and IRF was estimated to be $\leq$150 fs. For sub ps dynamic, the signal from the solvent system was recorded under same experimental conditions and placed in respective figures in the text for comparison where overlapping of solvent induced transient with transient signal from the sample is substantial. However, to minimize the solvent signal pump pulse energy was kept below 3 μJ per second and probe pulse energy was from 0.1–0.5 μJ at the sample. For transient absorption spectra the group velocity

Published on 31 luglio 2015. Downloaded by Fail Open on 23/07/2025 10:08:23.

dispersion compensation of white light continuum (probe beam) was done using studied solvent's two photon absorption data for few ps delay. All the samples were checked before and after taking the transient absorption to monitor the sample degradation if any.

Results and discussions

Synthesis

Synthetic schemes for preparing both the dyads are shown in Fig. 1. 4-(9,10-Dihydro-9,10-dioxoanthracen-6-yl)benzaldehyde (AQ-CHO) was achieved by condensation of 2-bromoanthraquinone with (4-formylphenyl)boronic acid. The starting material corrole phosphonium salt (TTC-CH_2-$PPh_3^+Br^-$) was synthesized according to the literature.[38] Both the dyads were synthesized by using Wittig–Horner reaction to create conjugation (double bond) between the β-pyrrole position of the corrole and either ferrocene or anthraquinone moieties.[46] Finally, the crude compound was purified by chromatography using a flash silica gel column. Both the dyads were found to be stable at room temperature. Preliminary characterization of the both dyads was carried out by ESI-MS and UV-Visible spectroscopic methods. The mass spectrum of both the dyads **Cor–Fc** and **Cor–AQ** showed peaks at m/z = 780 ($[M]^+$ + H, $C_{52}H_{42}FeN_4$) and 877 ($[M]^+$, $C_{62}H_{46}N_4O_2$) respectively, and are ascribable to the molecular-ion peak (S1 and S2 ESI†).

^{1}H-NMR spectral data of both the dyads have been summarized in the Experimental section and the spectra of **Cor–Fc** and **Cor–AQ** are shown in Fig. S3 (ESI†). Comparison of these spectra with those of individual constituents (**TTC**, **Fc-CHO** and **AQ-CHO**) reveals that there are certain specific changes in the peak positions of various protons present on the corrole macrocycle and that of its individual constituents. For example, the tolyl protons of corrole macrocycle split into two singlets in **Cor–Fc**. The singlet and doublet at 4.16 ppm; 4.26 ppm, respectively, belong to ferrocene protons. The two doublets appearing at 6.50 and 7.25 ppm belong to vinylic protons. This further confirms the formation of dyads. A similar set of peaks were observed in the **Cor–AQ** dyad.

Ground state properties

The electronic absorption spectra of the dyads **Cor–Fc** along with their constituent monomers in CH_2Cl_2 solvent are shown in Fig. 2. The wavelength of absorption maxima and molar extinction coefficients along with monomeric units are listed in Table 1. The monomeric component Fc-CHO shows a band at 220 nm due to Fe(a_{1g}) → Cp(e_{1g}) charge transfer whereas a peak in the 450 nm region due to symmetry forbidden Fe(a_{1g}) → Fe(e_{1g}) transitions (Fig. 2). In contrast, the monomeric component AQ-CHO shows a series of bands between 220 and 330 nm due to π–π* transitions (see ESI†). As shown in Fig. 2, the absorption spectra of the dyad is a mere superposition of the absorption spectra of monomers Ferrocene and corrole and it is dominated by corrole $S_0 \rightarrow S_1$ (Q-band) and $S_0 \rightarrow S_2$ (Soret band) transitions due to their high molar extinction coefficient. The introduction

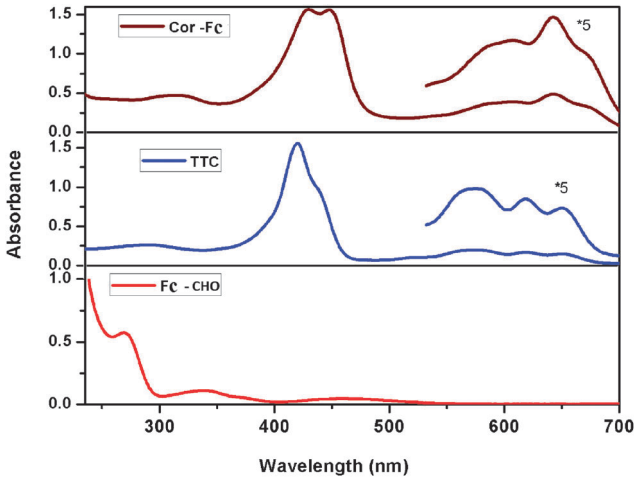

Fig. 2 Absorption behaviour of **TTC**, **Fc-CHO**, & **Cor–Fc** in CH_2Cl_2 at 0.01 mM concentration.

of ferrocene or anthraquinone at the β-pyrrole position of corrole results in the following changes of the absorption spectra: (a) a red-shift along with broadening and splitting of the Soret band (~10 nm); (b) a red-shift of the Q bands (~25 nm). The split in the Soret band and red-shift withdrawing bulky substituents at β-pyrrole of corrole absorption bands are probably due to the electron macrocycle, which deviate the planarity of the corrole macrocycle.[35] On the other hand Gryko *et al.* did not observe any π–π interactions when a ferrocene was attached at the *meso* position of a corrole.[47] The broadening is more pronounced in the longer wavelength region (>600 nm) (Fig. S4, ESI†) which might be due to the presence of donor–acceptor type of molecular arrangement which promotes charge delocalization and thus leads to ground state stabilization. In contrast, broadening can also be due to many conformers at different orientations of corrole units around the two –C═C– bonds. The observations of broadening, red-shift and split in the Soret band suggest a modest electronic interaction between the corrole π-system and the substituents either ferrocene or anthraquinone. Such changes were not observed for the absorption spectra for 1:1 equivalent mixture solution of corrole and ferrocene or anthaquinone (see Fig. S5, ESI†).

With a view to evaluate energies of the charge separation states (E_{CS}), which, as will be discussed in the later part of this paper, are useful quantities in analyzing the photochemical properties of these dyads, we have carried out electrochemical investigation using a differential pulse voltammetric technique. Fig. 3 depicts the differential pulse voltammograms of **TTC**, **Cor–Fc** and **Cor–AQ**. Table 1 summarises the redox potential data (CH_2Cl_2 and 0.1 M TBAP) of the D–A systems investigated in this study along with that of the corresponding individual constituents. From Fig. 3 and Table 1, both the dyads investigated under same experimental conditions show four oxidations and three reduction peaks. Wave analysis suggested that, while the first two reduction steps in **Cor–AQ** and first two oxidation steps in **Cor–Fc** are reversible (i_{pc}/i_{pa} = 60–70 mV; ΔE_p = 65 ± 3 mV for ferrocenium/ferrocene couple) reactions,

 This journal is © the Owner Societies 2015

Published on 31 luglio 2015. Downloaded by Fail Open on 23/07/2025 10:08:23.

Table 1 Absorption and electrochemical data

Compound	Absorption, λ_{max}, nm[a] ($\log \varepsilon$, M^{-1} cm^{-1})		Potential v *vs.* SCE[b]	
	Corrole-bands	Metallocene/quinone bands	Oxidation	Reduction
TTC	417(5.33), 572(4.39), 617(4.33), 650(4.27)	—	0.57, 0.84, 1.26, 1.80	−0.52, −1.74
AQ-CHO	—	283(4.32), 340(3.65)	—	−0.96, −1.38
Fc-CHO	—	269(3.59), 338(2.87), 460(2.5)	0.48	—
Cor–Fc	444(4.49), 426(4.50), 606(3.83), 642(3.93), 675(3.73)	260(3.95), 310(3.91)	0.69, 0.90, 1.25, 1.69	−0.60, −1.40
Cor–AQ	426(4.48), 448(4.45), 606(3.89), 639(3.95), 668 (3.80)	255(4.16), 302(4.10)	0.58, 0.81, 1.24, 1.77	−0.59, −1.04, −1.53

[a] Solvent CH_2Cl_2. Error limits: λ_{max}, ±1 nm; $\log \varepsilon$, ±10%. [b] CH_2Cl_2, 0.1 M TBAP. Glassy carbon working electrode; standard calomel electrode is the reference electrode, Pt electrode is the auxiliary electrode. Error limits, $E_{1/2}$ ± 0.03 V.

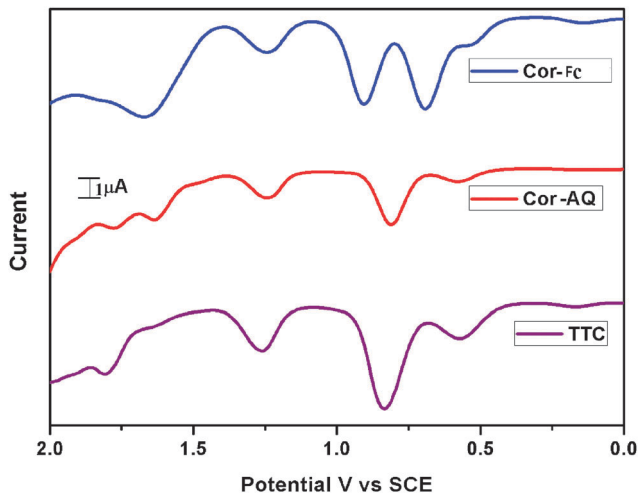

Fig. 3 Differential pulse voltammograms of **Cor–Fc**, **Cor–AQ** and **TTC** in CH_2Cl_2 with 0.1 M TBAP.

the subsequent steps are, in general, either quasi-reversible ($E_{pa} - E_{pc}$ = 90–200 mV and i_{pc}/i_{pa} = 0.5–0.8 in the scan rate (ν) range 100–500 mV s^{-1}) or totally irreversible. Fig. 4 and Table 1 also reveals that the electrochemical redox potentials of the both the dyads are slightly shifted as those of their corresponding monomeric analogues. For instance, the first reduction peak of **Cor–AQ** at −0.59 V belongs to the corrole part of the dyad whereas the second reduction at −1.04 belongs to the anthraquinone part of the dyad as in the case of their monomeric units it appeared at −0.52 and −0.96 V for corrole and anthraquinone, respectively.

To distinguish the redox potentials of these dyads spectroelectrochemistry was carried out under same solution conditions as per differential pulse voltammetry measurements. Upon the first controlled potential reduction of **Cor–AQ** at −0.70 V, the intensity of the the Soret band at 426 nm decreases while being red-shifted to 446 nm as shown in Fig. 4, while the Q band at 637 nm also gets red-shifted to 678 nm with its intensity increasing. During this process isosbestic points were observed at 313, 355, 523, and 647 nm. The intensity of the newly formed band at 678 nm further increases with the third controlled reduction potential at −1.70 V. The step-wise reduction products are assigned as π-anion and dianion radicals.[48] No spectral changes were observed when reduction potential is controlled at −1.30 V. This is probably due to the reduction of anthraquinone at this potential. The spectral changes obtained during first and second oxidations are illustrated in Fig. 4. Upon controlled oxidation potential at 0.70 V, the Soret band at 423 nm decreases its intensity with a red-shift to 465 nm. Whereas the Q band at 635 nm decreases its intensity with the formation of a new band at 714 nm. During this process isosbestic points are observed at 469 and 684 nm. The new band at 714 nm further increases its intensity when controlled potential is shifted to 1.05 V. Similar spectra have been assigned to corrole cation radicals, and a π-cation radical is assigned in the present study.[49] We have not observed any oxidation wave of (AQ) under the experimental conditions employed. Therefore the oxidation waves belong to purely the corrole part of the **Cor–AQ** dyad.

Spectral changes of **Cor–Fc** upon controlled reduction potential at −1.75 V are illustrated in Fig. 5. The Soret band at 423 nm was red-shifted to 437 nm with a change in intensity of the band. Whereas the Q band at 640 nm decreases its intensity with the formation of a new band at 668 nm. During this process isosbestic points were observed at 456, 518 and 648 nm. The reduction product was assigned as the π-anion radical as there was no reduction observed in Ferrocene. When the controlled potential shifted to 0.75 V, the Soret band decreases its intensity and red-shifted to 431 nm, while the intensity of the Q band at 642 nm reduces with formation a new band at 715 nm. The intensity of the newly formed band then decreases upon second controlled potential oxidation at 1.10 V. The step-wise oxidation products are assigned as the π-cation radical and the dication.

Theoretical calculations

In order to examine the nature and position of frontier molecular orbitals, density functional theory (DFT) calculations have been carried out.[44] Complete optimization without any constraint was done using B3LYP and 6-31g(d) basis sets to see the structural parameters of the two systems, **Cor–Fc** and **Cor–AQ**. Fig. 6 displays the HOMO and LUMO distribution and geometrical optimized structures of the dyads obtained by DFT calculations. From Fig. 6, it is clear that the HOMO is mainly distributed at the corrole moiety while LUMO was mainly distributed at the anthraquinone moiety in **Cor–AQ**. Whereas in **Cor–Fer**, the HOMO−1 is distributed among corrole and ferrocene moieties of the dyad and LUMO is distributed mainly on corrole (Fig. 6). The energies of HOMO and LUMO for dyads **Cor–AQ** and **Cor–Fc** were found to be −4.56 & −4.85 eV and

Published on 31 luglio 2015. Downloaded by Fail Open on 23/07/2025 10:08:23.

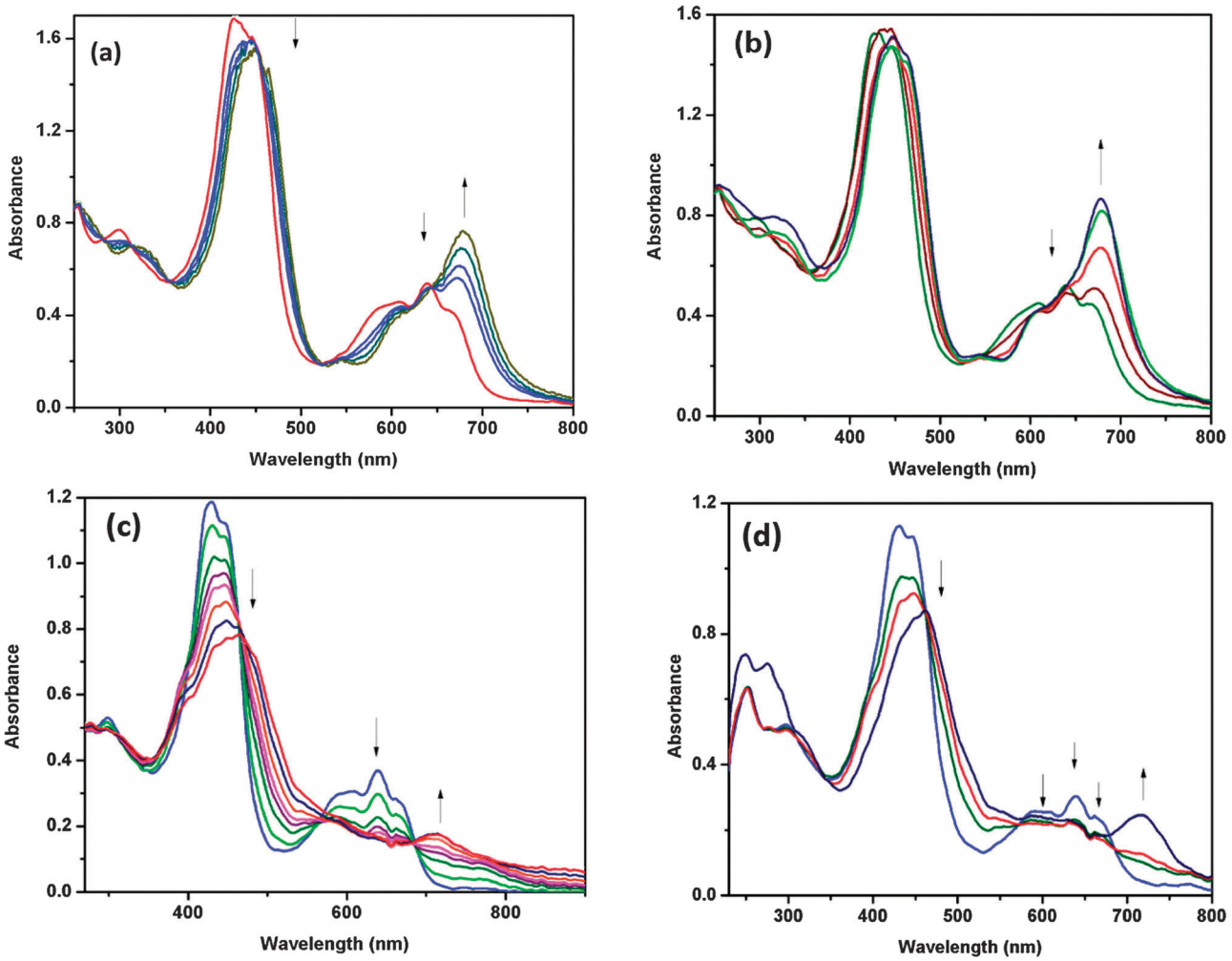

Fig. 4 *In situ* UV-Visible spectroelectrochemical changes of (**Cor–AQ**) at an applied redox potential (a) −0.70 V, (b) −1.70 V, (c) +0.70 V and (d) +1.05 V, using SCE as the reference electrode.

−2.71 & −2.15 eV, respectively. From the geometrical optimized structures (Fig. S10 and S11, ESI†), in both the dyads the corrole macrocycle and either anthraquinone or ferrocene are far apart. Moreover, phenyl rings at *meso* positions are found to be perpendicular to the plane of the corrole ring, which prevents the stacking interaction. All these observations corroborate the prevalence of the *through-bond* intramolecular electron transfer mechanism in the current systems.

Singlet state properties

Unlike the case with the ground state properties, major differences have been noticed in the singlet state properties of both the dyads. Steady-state fluorescence emission spectra of both the dyads have been measured in four different solvents (hexane, dichloromethane, acetonitrile and DMF) with change of polarity and compared with constituent fluorescence emission spectra of **TTC** in corresponding solvent as shown in Fig. 7. The corresponding singlet state data were presented in Table 2. The fluorescence emission maxima (λ_{em}) of both the dyads are red-shifted, when compared to its reference compound TTC in all investigated solvents (λ_{ex} = 425 nm). A similar kind of red-shifted fluorescence emission behaviour was also observed in other β-pyrrole substituted corroles.[28] The red-shift of the fluorescence emission spectra of both dyads is presumably due to increased polarity of the emitting state originated from the donor–acceptor (D–A) type of molecular arrangement. Interestingly, we observe a remarkable quench in corrole emission intensity when equi-absorbing solutions of dyads were excited at 425 nm (λ_{max}, where corrole absorbs predominantly). The possibility of self-aggregation of corroles which leads to quenching of fluorescence intensity (as a result of non radiative path in the excited state) can be ruled out as all experiments were carried out with very dilute solutions (10^{-6} M). Moreover, we could not observe substantial changes in the absorption spectra as it happens in few corrole systems.

Various radiative and non-radiative intramolecular processes can be conceived to participate in the excited state decay of **Cor–Fc** & **Cor–AQ**. Among these, an excitation energy transfer (EET) or photoinduced electron transfer (PET) can be assumed to participate in the quenching of fluorescence emission intensity. For EET, the emission spectrum of donor has to be overlapped with the absorption of the acceptor. It is evident from

 This journal is © the Owner Societies 2015

Published on 31 luglio 2015. Downloaded by Fail Open on 23/07/2025 10:08:23.

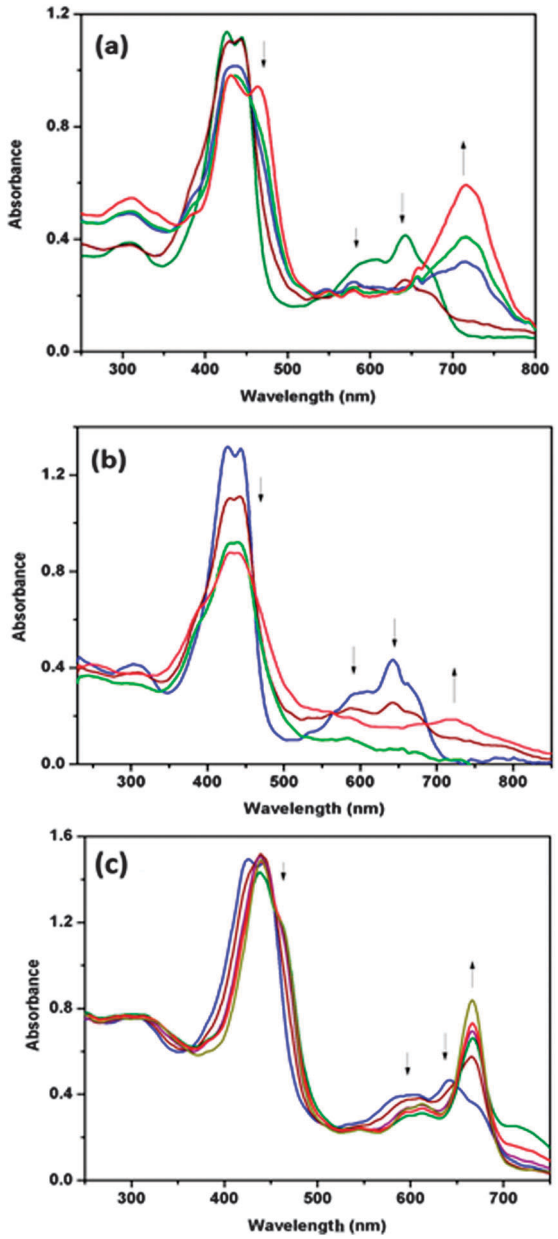

Fig. 5 *In situ* UV-Visible spectroelectrochemical changes of **Cor–Fc** at an applied redox potential (a) +0.75 V, (b) +1.1 V, and (c) −1.75 V, using SCE as the reference electrode.

Fig. 2 and 7 that the EET is not possible between corrole and either anthraquinone or ferrocene due to the lack of proper spectral overlap. An alternative pathway for emission quenching is the intramolecular PET. The E_{00} (0–0 spectroscopic transition energy) values of the corrole part of dyads, 1.89 ± 0.05 eV, 1.90 ± 0.05 eV for **Cor–Fc** and **Cor–AQ**, respectively as estimated from overlap of their absorption and emission spectra were found to be in the same range as the E_{0-0} values of free TTC.[38] When excited at 425 nm, the singlet excited state of corrole either can donate an electron to an energetically favourable acceptor (oxidative electron transfer) or can take an electron from a suitable donor (reductive electron transfer). The change in free energy for PET from the corrole to the anthraquinone in **Cor–AQ** can be calculated using eqn (1).

$$\Delta G^{\circ}(1\mathrm{Cor} \rightarrow \mathrm{AQ}) = e[E(\mathrm{Cor}^{*}/\mathrm{Cor}^{\bullet+}) - E(\mathrm{AQ}/\mathrm{AQ}^{\bullet-}) - E_{00}(\mathrm{Cor})] \quad (1)$$

ΔG° was found to be −0.73 eV when excited at 425 nm. Whereas in the case of **Cor–Fc**, the change in free energy for a PET reaction from ground state of ferrocene to singlet state of corroles was found to be −0.60 eV. A PET reaction from the singlet state of corrole to the ground state of ferrocene thermodynamically is not feasible (ΔG° was found to be 0.59 eV).

Fluorescence quantum yields of the dyads and individual constituents have been estimated (Table 2) by comparing the emission spectra of the reference compound (*i.e.*, TTC (ϕ) = 0.21 in toluene) with that of the dyads.[29] It was found that the fluorescence quantum yield (ϕ) of **Cor–Fc** and **Cor–AQ** was 0.012 and 0.013, respectively in CH_2Cl_2. The fluorescence quenching efficiency (Q) of the dyads was calculated by eqn (2).

$$Q = \frac{\phi_{\mathrm{TTC}} - \phi_{\mathrm{Dyad}}}{\phi_{\mathrm{TTC}}} \quad (2)$$

Where ϕ_{TTC} refer to the fluorescence quantum yields for tritolyl corrole and ϕ_{Dyad} refer to (**Cor–Fc**) or (**Cor–AQ**); (λ_{ex} = 425 nm). As the static dielectric constant of the solvent is increased, the quenching of fluorescence intensity increased gradually (Table 2), indicating the excited state electron transfer mechanism. For example, quenching efficiencies in hexane are less compared to CH_2Cl_2, CH_3CN and DMF. In general, the PET process is accelerated in polar solvents than in non-polar solvents, so the present results are in consistent with the literature.[39] In all investigated solvents, the efficient quenching of the **Cor–AQ** dyad relative to that of the **Cor–Fc** dyad can be directly attributed to the more exothermic value of ΔG_{PET} of **Cor–AQ**.

Femtosecond time resolved fluorescence

Further evidence of the intramolecular PET process has been determined by measuring the excited state decay curves. The fluorescence decay of the **TTC** in ACN is measured by TCSPC and is found to be monoexponential with a 3.5 ns lifetime.[29] On the other hand, the fluorescence dynamics of the dyads was observed to be too fast to be properly resolved by TCSPC in any of the solvents studied and was thus measured by the femtosecond time-resolved fluorescence up-conversion (FU) technique. However, to compare the extent of singlet-state quenching of corrole in the dyads, fluorescence decay was measured for **TTC**, **Cor–Fc** and **Cor–AQ** in ACN in a 10 ps time window. Fig. 8 shows the FU time profiles of **TTC**, **Cor–Fc** and **Cor–AQ** in ACN at 670 nm upon 410 nm excitation. The FU signal profile of **TTC** at 670 nm exhibits a biphasic decay and is well fit with 3 ps and a lifetime that is too long to be measured exactly using this equipment but is consistent with the lifetime of the S1 state of **TTC** 3.5 ns. The fit curve is shown in Fig. 8 and corresponding amplitudes are listed in Table 3. In analogy to the ultrafast dynamics of tetrapyrrolic systems reported elsewhere[45,50,51] the first component can be assigned to the vibrational cooling

Published on 31 luglio 2015. Downloaded by Fail Open on 23/07/2025 10:08:23.

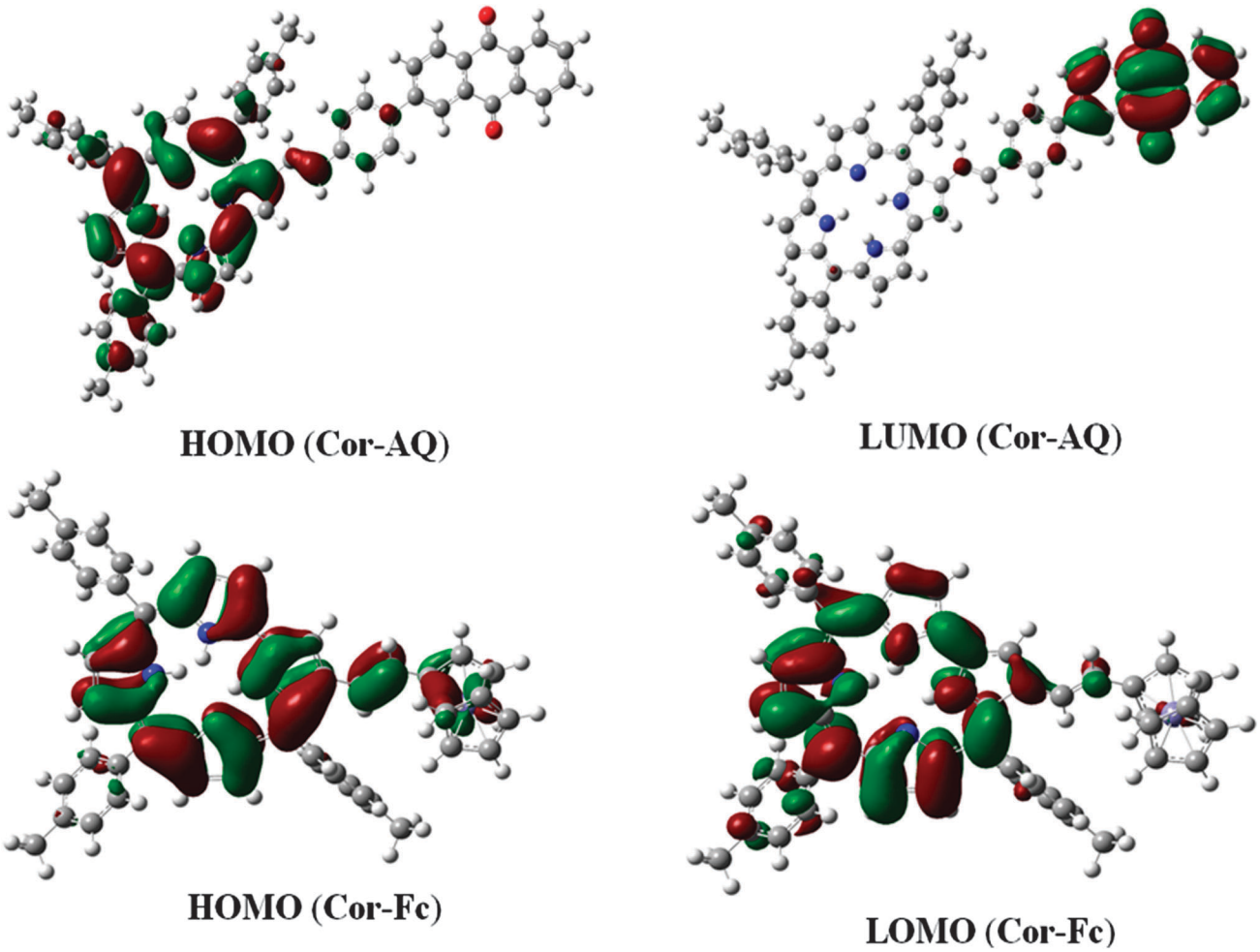

Fig. 6 HOMO–LUMO of **Cor–AQ** (above), and HOMO–LUMO of **Cor–Fc** (below).

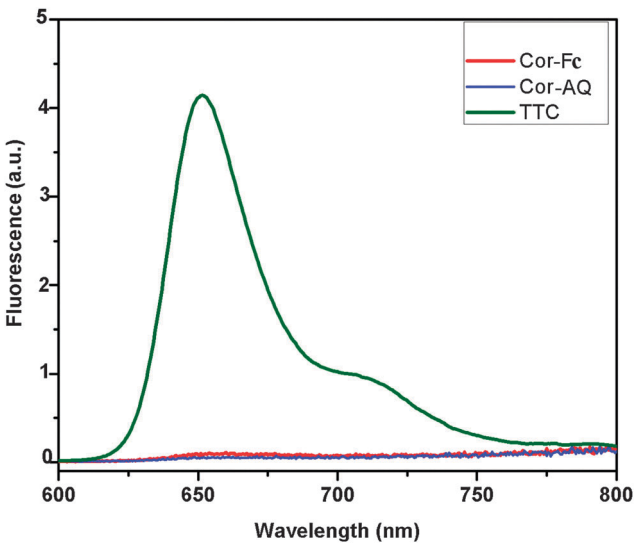

Fig. 7 Fluorescence spectra of **Cor–Fc**, **Cor–AQ** and **TTC** at λ_{ex} = 425 nm in acetonitrile equi-absorbing solutions (O.D. λ_{ex} = 0.05).

processes. However, the FU signal profile of the **Cor–AQ** dyad shows a very fast decay and it is nicely fit by bi-exponential components with 2 ps lifetime, a major component, along with a very weak and long 3 ns lifetime which was kept as constrained. The 2 ps component for this dyad is assigned to be due to charge separation (CS) resulting from electron transfer from the singlet excited state of corrole to anthraquinone part of the dyad. Fig. 8 also shows the FU signal profile of the **Cor–Fc** dyad and it can be analysed with three-exponential decay components and the lifetime values of first two components were found to be 2.5 ps and 355 ps whereas the lifetime of the third component was kept constant at 3 ns, the lifetime of free **TTC**. As shown in Table 3, 95% of the decay processes are covered by first two components and the third component is only 5%. The weighted average of first two components was found to be 36 ps and it is assigned to be the charge separation (CS) time due to electron transfer from ferrocene to the singlet excited state of corrole. The quantum yield of charge separation, φCS, is calculated using eqn (3) and found to be >99% for **Cor–AQ** and >98% for **Cor–Fc** which are in good agreement with the steady state quenching data (Table 2).

$$\Phi_{CS} = \frac{(1/\tau_{CS})_{Dyad} - (1/\tau_f)_{TTC}}{(1/\tau_f)_{TTC}} \quad (3)$$

 This journal is © the Owner Societies 2015

Published on 31 luglio 2015. Downloaded by Fail Open on 23/07/2025 10:08:23.

Table 2 Steady state emission data

	λ_{em}, nm[a,b] (ϕ, %Q), λ_{ex} = 425 nm			
Compound	Hexane	CH_2Cl_2	CH_3CN	DMF
TTC	671 (0.29)	674 (0.25)	651 (0.24)	655 (0.29)
Cor–Fc	688 (0.012, 95)	690 (0.012, 95)	663 (0.014, 94)	668 (0.012, 96)
Cor–AQ	680 (0.13, 95)	683 (0.013, 95)	656 (0.012, 95)	664 (0.01, 97)

[a] Error limits: λ_{ex}, ±2 nm, ϕ ± 10%. [b] Q is defined in eqn (2) (see text).

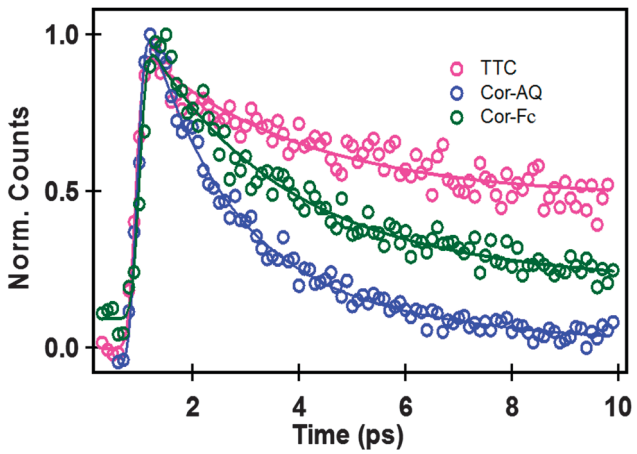

Fig. 8 Time profile of fluorescence up-conversion signal of **TTC**, **Cor–AQ**, and **Cor–Fc** dyads upon 410 nm excitations in acetonitrile solvent.

Table 3 Kinetic parameters of fluorescence up-conversion data analysis

Signal	λ_{Probe} (nm)	1st component τ_1 (ps), A_1 (%)	2nd component τ_2 (ps), A_2	3rd component ($\tau_3 \equiv 3.5$ ns), A_3 (%)	CS (ps)
TTC	670	3, 47	—	53	—
Cor–AQ	670	2 ± 0.5, 98	—	2	2
Cor–Fc	670	2.5 ± 0.2, 85	355 ± 90, 9%	6	36[a]

[a] Weighted average of 1st and 2nd components $\left(\tau_{avg} = \frac{(\tau_1 \times A_1 + \tau_2 \times A_2)}{(A_1 + A_2)}\right)$.

Furthermore, the rate constant (k_{ET}) for the charge transfer state $Cor^{-\bullet}Fc^{+\bullet}$ and $Cor^{+\bullet}$–$AQ^{-\bullet}$ has been calculated using eqn (4) and is accounted below.

$$k_{ET} = (1/\tau_f) - k \quad (4)$$

where k is the reciprocal of the lifetime of the TTC, τ_f is the lifetime of **Cor–Fc** and **Cor–AQ**. The rate constant values for **Cor–Fc** and **Cor–AQ** were found to be 2.78×10^{10} and 3.33×10^{11} s^{-1}, respectively. Overall, the photoinduced reactions are influenced by the nature of the substituent which is connected to the corrole macrocycle. Both in steady-state and excited state lifetime, the quenching was higher for the anthraquinone dyad than its corresponding ferrocene dyad. This might be due to the more electron withdrawing nature of anthraquinone and this is reflected in electrochemical studies (Table 1). The observed CS is faster for **Cor–AQ** than for **Cor–Fc** in acetonitrile and it can be easily rationalized by considering the thermodynamic driving force which is 0.13 eV larger for the **Cor–AQ** dyad. In terms of Marcus theory,[52] CS in these dyads is moderately exergonic (−0.60 to −0.73 eV) and takes place in the normal regime. As a result its rate constant increases with the driving force.

Femtosecond time resolved absorption spectra

In the view to detect the radical anion/cation we have measured transient absorption (TA) spectra of TTC along with **Cor–Fc** and **Cor–AQ** in ACN upon Soret (410 nm) as well as Q band (575 nm) excitations. Fig. 9 shows the typical transient absorption spectra of TTC in ACN when excited upon 410 nm (Fig. S13, ESI,† upon 575 nm excitation) and it is quite similar to that of the well studied tetrapyrrolic system TPP.[53] The spectra exhibits two negative bands corresponding to Soret and Q band absorption centered around 420 and 560 nm and they can be assigned to the ground state bleaching (GSB) of $S_0 \rightarrow S_2$ and $S_0 \rightarrow S_1$ respectively. A strong positive signal in between 450 to 560 nm can be assigned to excited state absorption (ESA), $S_n \leftarrow S_1$ transition. The dynamic features of the transient absorption were analyzed at three different wavelengths 420, 460 and 575 nm in three different time windows of 10 ps, 100 ps and 6 ns and they are shown in Fig. 10 and Fig. S14 and S15 (ESI†). The temporal evolution of all transient absorption data can be well fit with three sets of lifetime values, 0.5 ± 0.1 ps (τ_1), 3 ± 1 ps (τ_2) and a lifetime (τ_3) that is too long to be measured with our existing femtosecond system but this long lifetime value is very consistent with the S_1 fluorescence lifetime of 3.5 ns, measured by the TCSPC method. The fit curves are shown in Fig. 10 where the above set of lifetime values were used as constrained to fit the data. Component amplitude values are listed in Table 4.

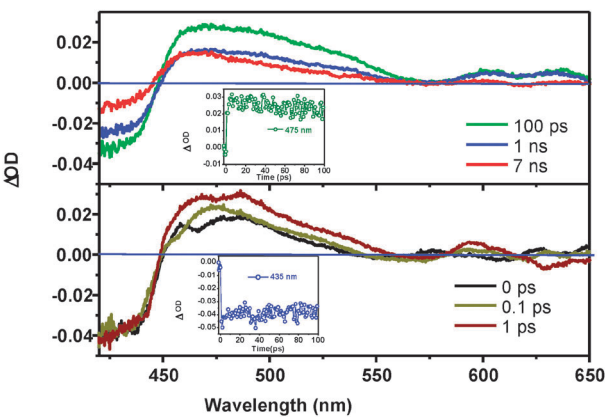

Fig. 9 Transient absorption spectra measured at several time delays after $S_2 \leftarrow S_0$ excitation at 410 nm of **TTC** in ACN. Inset shows the decay profiles of TA at respective wavelengths.

Published on 31 luglio 2015. Downloaded by Fail Open on 23/07/2025 10:08:23.

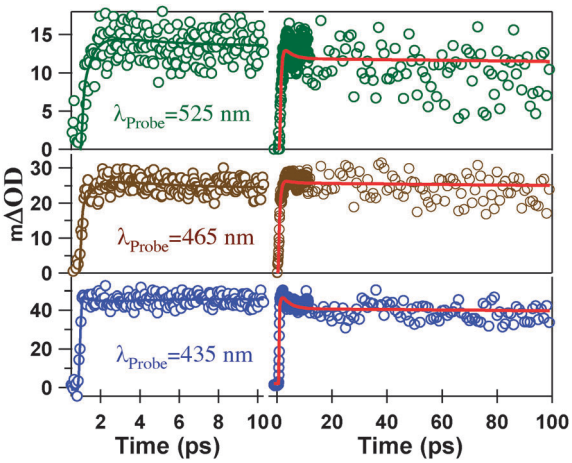

Fig. 10 Femtosecond transient absorbance of TTC in ACN. Pump wavelength was 410 nm and probe wavelengths were as shown. The ground state bleaching signal at 435 nm has been inversed to easily compare with transient absorption of singlet excited states. Solid red lines are fits of the experimental data using a common set of lifetimes (see text). Solid lines in 10 ps data are fits to estimate ultrafast components, τ_1 and τ_2.

Table 4 Component relative amplitudes of fits of transient absorption measurements for 410 and 575 nm excitation of **TTC** in ACN

λ_{Probe} (nm)	1st component ($\tau_1 \equiv 0.5 \pm 0.1$ ps) A_1 (%)	2nd component ($\tau_2 \equiv 3 \pm 1$ ps) A_2 (%)	3rd component ($\tau_3 \equiv 3.5$ ns) A_3 (%)
435	−20	25	75
	—	—	100[a]
465	−100	6	94
	—	—	100[a]
525	−100	21	79
	—	—	100[a]

[a] Amplitude corresponds to the mono-exponential fit to the transient absorption signal upon Q band excitation. A negative component indicates the respective component is rise instead of decay.

The similar sets of temporal evolution of TA signals upon 575 nm excitation were also analysed and found to be mono-exponential decay with 3.5 ns lifetime values (Fig. S14 and S15, ESI†). It is important to note here that $T_n \leftarrow T_1$ absorption of **TTC** is comparable to that of $S_n \leftarrow S_1$ in the wavelength range probed,[54,55] the population dynamics for equilibrated S_1 and T_1 are effectively combined in a long-lived 3.5 ns component for both S_2 & S_1 excitations for this experimental time window. The disappearance of the first two components from the TA signal upon Q band excitation clearly points to the fact that they are related with the ultrafast relaxation process when TTC is excited at S_2. The first component of the transient decay profile of the ESA signal at 465 and 525 nm upon S_2 excitation was found to be the rise component with a lifetime value of 0.5 ps and it was found to be the partial rise component in the ground state bleaching signal. This ultrafast shortest component can be ascribed to $S_1 \leftarrow S_2$ internal conversion. The second and third components for both ESA and ground state bleaching signals were decay components and they correspond nicely to the fluorescence up-conversion signal. Hence these components can be ascribed as vibrational cooling (3 ps) and S_1 lifetime *i.e.*, S_1 state population decay to the ground state or intersystem crossing to the triplet state (T_1) of **TTC**.

Transient absorptions are measured at several delays after S_2 and S_1 excitations at 410 and 575 nm respectively for both the dyads, **Cor–AQ** and **Cor–Fc** in ACN and they are shown in Fig. 11A and B and Fig. S16 (ESI†) (575 nm excitation). TA spectra for both the dyads composed of negative signals centered around 435 nm corresponding to the S_2 ground state absorption and positive signal peaking around 485 nm but above 570 nm signals are too weak to be resolved. The overall shape of TA spectra for both the dyads is more or less similar to that of TTC apart from a systematic ~20 nm red shift of the peak position of transient absorption of excited states and the ground state bleaching band. Interestingly, the ΔOD values of either ground state bleaching or the transient absorption of singlet excited states is remarkably lower than that of TTC, when concentration of the studied systems and the pump laser power were kept same. No distinct excitation dependent change in TA absorption spectra was observed for these two dyads. However, the intensity of TA spectra reduces to zero within 20 ps for the **Cor–AQ** dyad and 200 ps for **Cor–Fc**. No distinct absorption spectra for corrole

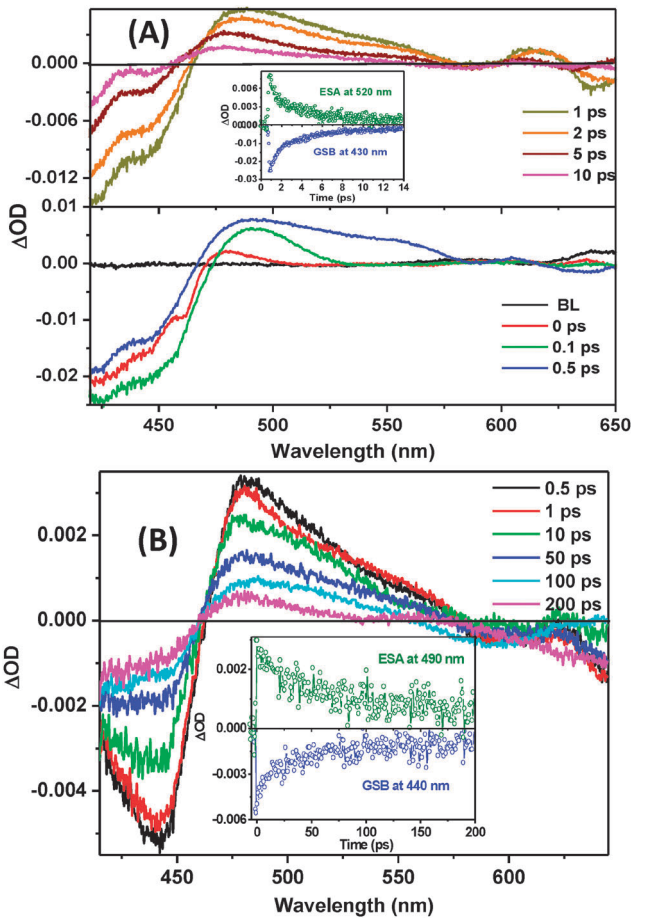

Fig. 11 Transient absorption spectra of **Cor–AQ**, λ_{ex} = 410 nm (A) and **Cor–Fc** (B) in ACN. Insets show typical excited state absorption and ground state bleaching profiles of respective dyads.

This journal is © the Owner Societies 2015

Published on 31 luglio 2015. Downloaded by Fail Open on 23/07/2025 10:08:23.

anion or corrole cation were detected but a trend of blue shift of the peak position of transient absorption of singlet excited states was observed on increasing the delay time. Temporal evolution of transient absorption strongly depends on the probe wavelength. The transient absorption kinetics have different profiles at different wavelengths of TA spectra (Fig. S17, ESI†) and the TA profile at around peak position is complex in nature and very difficult to fit convincingly. However, the TA signal profile above the 500 nm probe wavelength is quite simple and it follows the dynamic as to the fluorescence decay profile quite satisfactorily. A comparative decay profile of transient absorption signals at 515 nm probe wavelength upon two different excitations with fluorescence decay profile at 670 nm is shown in Fig. S18 and S19 (ESI†) for **Cor–AQ** and **Cor–Fc** dyads, respectively. However, the TA profile above 500 nm for both the dyads can nicely fit the three components, of which first two components contribute 80–90% of the decay and rest is contributed by the third component whose lifetime (3.5 ns) is consistent with the S_1 decay of **TTC** and kept constant for the fitting (Fig. 12). The fitting parameters are listed in Table 5 for both the excitations. The weighted average of first two decay times nicely corresponds to the fluorescence decay of the S_1 state of dyads and it is ascribed to the CS state.

The absorption spectrum of the radical anion of TPP/Zn-TPP, a typical tetrapyrrolic system, is composed of an intense Soret band red shifted by 10–20 nm than that of parent systems and a much weaker band just after Q band of the neutral parent system.[56] Similarly, the absorption spectrum of the radical cation of those systems do not differ much, with an intense band peaking after the Soret band of the neutral system and a weak and broad one after the Q band of the neutral system. TTC being a similar kind of tetrapyrolic system, the characteristic absorption spectra of its radical anion or radical cation should contain an intense band between 440 nm and 470 nm. As a consequence, in the case of the PET event in **Cor–Fc** or **Cor–AQ** dyads a clear absorption band was expected in TA absorption spectra between

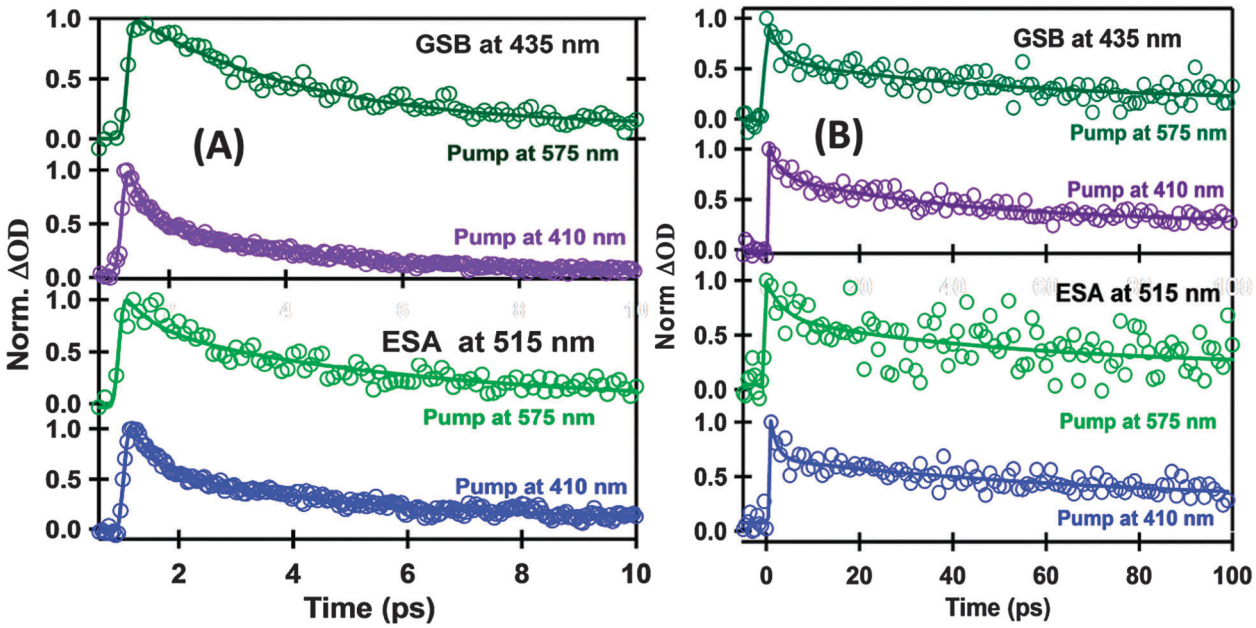

Fig. 12 Kinetic profile of excited state absorption at 515 nm (lower panel) ground state bleaching at 435 nm (upper panel) upon 410 and 575 nm excitation of **Cor–AQ** (A) **Cor–Fc** (B) in ACN.

Table 5 Component relative amplitudes of fits of transient absorption measurements for 410 and 575 nm excitation of **Cor–AQ** and **Cor–Fc** in ACN

Dyad	Signal	λ_{Pump} (nm)	λ_{Probe} (nm)	1st comp. τ_1 (ps), A_1 (%)	2nd comp. τ_2 (ps), A_2 (%)	3rd comp. ($\tau_3 \equiv 3.5$ ns), A_3 (%)	CS/CR (ps)
Cor–AQ	ESA	410	515	0.5 ± 0.05, 50	3.7 ± 0.3, 46	4	2[a] (CS)
		575	515	1.9 ± 0.1, 46	3.1 ± 0.1, 45	9	2.5[a] (CS)
	GSB	410	435	0.25 ± 0.05, 48	2.9 ± 0.1, 49	3	1.6[a] (CR)
		575	435	—	3.0 ± 0.1, 94	6	3[a] (CR)
Cor–Fc	ESA	410	515	3.5 ± 0.2, 36	53 ± 2, 46	18	32[a] (CS)
		575	515	1.5 ± 0.1, 50	73 ± 3, 40	10	33[a] (CS)
	GSB	410	435	2.6 ± 0.2, 42	55 ± 2, 48	10	31[a] (CR)
		575	435	2.5 ± 0.2, 30	53 ± 2, 55	15	35[a] (CR)

CS – charge separation, CR – charge recombination. [a] Weighted average of 1st and 2nd components $\left(\tau_{avg} = \frac{(\tau_1 \times A_1 + \tau_2 \times A_2)}{(A_1 + A_2)}\right)$.

Published on 31 luglio 2015. Downloaded by Fail Open on 23/07/2025 10:08:23.

440 nm and 470 nm as signature of the radical anion or radical cation formation respectively. However, TA spectra of neither **Cor–AQ** nor **Cor–Fc** show a clear absorption of respective ions but change of the peak position of transient absorption of singlet excited states as a function of time and a sharp different time evolution of positive transient signals below 500 nm. This observation reveals that TA absorption between 460 and 480 nm is the sum of absorption of radical ions and absorption of excited states and the decay of radical ions (charge recombination, CR) more or less follow the decay of transient absorption of singlet excited states. In the view to estimate the CR time, we have analyzed the ground state bleaching signals at 435 nm for both the dyads upon S_2 and Q band excitations and are shown in Fig. 12. Like the decay of transient absorption of singlet excited state decay, ground state bleaching profiles fit well by three components with short lifetime values and a long 3.5 ns component which was considered to be constraint of fitting. Resultant lifetime values of fitting analysis and corresponding amplitudes are placed in Table 5. Considering first two short components are due to the charge recombination to the vibrationally hot ground state, the average time constant to CR is calculated to be 2–3 ps for **Cor–AQ** and 31–35 ps for **Cor–Fc**. Hence, respective CS and CR are found to be almost equal for both the dyads resulting in non visibility of radical anion or cation spectra in TA spectra. In such circumstances, the observed CS population is leveled off due to CR as rise time of the CS band corresponds to the CR time constant and decay time of CS is the CS time constant itself. A similar situation was encountered by Vauthey et al for the porphyrin based system.[57] It is also important to mention that, CS and CR states are independent of the excitation wavelength and this observation clearly reveals that electron transfer occurs in thermal equilibrium singlet state of corrole for both the dyads.

To enumerate the spectra and associated lifetimes of the states, we carried out global analysis[58] on the TA data of both dyads in ACN using the Glotaran software[59] applying a sequential model resulting in evolution associated difference spectra (EADS). Since, the sequential model was used here to analyse TA data globally, the appeared EADS could represent a mixture of photophysical processes but one physical process dominated a particular lifetime. Fig. 13A and B show the normalized EADS resulting from the global fit of the data for both the dyads (for absolute EADS see Fig. S21, ESI†). At least three exponential functions are necessary to fit globally both the dyads and corresponding time constant nicely corroborated to the values obtained from the analysis of individual time profile of transient absorption of singlet excited states and ground state bleaching. The time constant of the first component ($EADS_1$) coincides with the major component of fluorescence decay of the dyads as observed in the FU study. Not only that, the spectral shape of the $EADS_1$ nicely corroborates to the TA spectra of simple TTC (Fig. S22, ESI†). Hence, $EADS_1$ can be assured to resemble the excited state spectra and the origin of the CS state. Since, a recombination channel of singlet states to the ground state occurs in parallel to charge separation, the time constant of $EADS_1$ obtained in this analysis presumably represents the lower limit

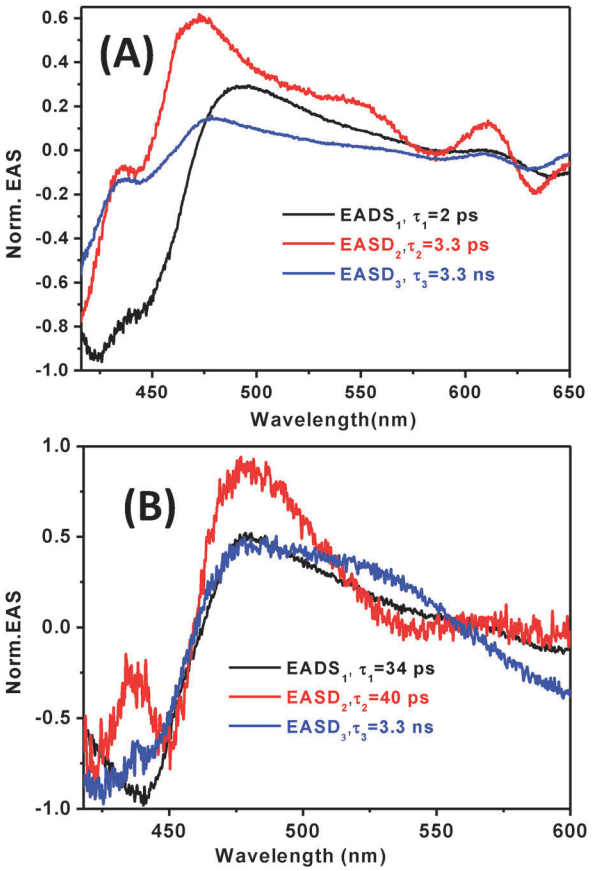

Fig. 13 Normalized evolution-associated difference spectra (EADS) resulting from global fitting applying a sequential model to the femtosecond transient absorption data of **Cor–AQ** (A) and **Cor–Fc** (B).

of charge separation time and it is found to be 2 ps for **Cor–AQ** and 34 ps for **Cor–Fc** respectively. The second component which has a slightly higher time constant of 3.3 ps for **Cor–AQ** and 40 ps for **Cor–Fc** reflects the CS state and associated $EADS_2$ could predominantly correspond to the absorption spectra of respective radical ions of the dyads. As shown in Fig. 13, the spectral shape of $EADS_2$ is clearly different from that of $EADS_1$. A new band in $EADS_2$ is observed at around 464 nm for **Cor–AQ** and at 437 nm for **Cor–Fc** dyads. This new band in $EADS_2$ for respective dyads can be attributed to one of the peak of the absorption spectra of the TTC radical cation and TTC radical anion respectively. The third longest time constant is very much same for both the dyads and also very close to the S_1 fluorescence lifetime of TTC measured by TCSPC and corresponding $EADS_3$ indicates that the S_1 state population decays directly to the ground state or to the nearest triplet state (T_1). The shape of the $EADS_3$ for both the dyads closely resemble the shape of $EADS_1$ with little blue shift of the excited state absorption peak and this can be ascribed to some contribution of $T_n \leftarrow T_1$ transition to the $S_n \leftarrow S_1$ transition in this long time scale.

Overall, the aforesaid results unambiguously point to the following facts: (a) occurrence of CS state for both the dyads, (b) the CS state is faster in **Cor–AQ** than in **Cor–Fc** by more than one order, (c) CS and CR states occur essentially with same time

 This journal is © the Owner Societies 2015

Published on 31 luglio 2015. Downloaded by Fail Open on 23/07/2025 10:08:23.

constants for the respective dyads. The free energy change for the CR calculated as $\Delta G_{CR} = E_{red}(\text{acceptor}) - E_{ox}(\text{donor})$, found to be −1.17 and −1.30 eV for **Cor–AQ** and **Cor–Fc** dyads respectively. Hence, it could apparently be concluded that the CR rate decreases on increasing free energy and CR occurs in the Marcus Inverted region. However, the total reorganization energy (λ) of tetrapyrrolic systems was found to be of the order of 1–1.5 eV.[60] So, for both the dyads $-\Delta G_{CR}$ tends to be equal to λ, and CR occurs in the Marcus optimal region, *i.e.* CR in both the dyads is essentially barrierless and the rate of CR is thus ultrafast in nature. Since CR is a barrier less process, its rate eventually is determined by the CS rate. The CS and, therefore, CR in **Cor–AQ** occurs in a 1–3 ps timescale which is very similar to the solvation in acetonitrile.[61] In such a case, both CS and CR processes are probably controlled by the dielectric response of the solvents leading to similar dynamics for CS and CR.[62]

Conclusions

We have designed and synthesized donor–acceptor system based corrole–anthraquinone and corrole–ferrocene dyads using a vinylic spacer. Both the dyads have been characterized by using various analytical tools. The ground state properties indicate modest interactions between corrole macrocycle and either anthraquinone or ferrocene moieties in both the dyads. Steady-state and fluorescence up-conversion studies revealed that **Cor–AQ** undergoes rapid electron transfer from the singlet state of corrole to anthraquinone and from the ground state of ferrocene to the first excited state of corrole in **Cor–Fc**. The electron transfer rates (or charge separation rates) for **Cor–Fc** and **Cor–AQ** were found to be 2.78×10^{10} and 3.33×10^{11} s^{-1}, respectively in acetonitrile solvent. Transient absorption studies indicate that respective charge separation and charge recombination occur in the same timescale for both the dyads. Due to a small energy gap between the charge separated state and the ground state, back electron transfer is a barrier-less process and occurs too fast. These results also establish corrole as an electron donor as well as an electron acceptor depending upon the nature of the other attached moiety.

Acknowledgements

We are grateful to the Department of Science and Technology (DST, SB/S1/IC-14/2014) for financial support of this work. The author KS acknowledges University Grants Commission (UGC) for Senior Research Fellowship (SRF). PRB acknowledge P. Hemant Kumar for helping to collect fluorescence up-conversion as well as transient absorption data. We also thank Joris Snellenburg for seminal support in the usage of the Glotaran software.

Notes and references

1 A. C. Fahrenbach, C. J. Bruns, H. Li, A. Trabolsi, A. Coskun and A. F. Stoddart, *Acc. Chem. Res.*, 2014, **47**, 482–493.
2 B. K. C. Chandra, G. N. Lim, V. N. Nesterov, P. A. Karr and F. D'Souza, *Chem. – Eur. J.*, 2014, **20**, 1–14.
3 L. Yuan, W. Lin, K. Zheng and S. Zhu, *Acc. Chem. Res.*, 2013, **46**, 1462–1473.
4 J. H. Kim, M. Lee, J. S. Lee and Ch. B. Park, *Angew. Chem., Int. Ed.*, 2012, **51**, 517–520.
5 D. Gust, T. A. Moore and A. L. Moore, *Acc. Chem. Res.*, 2009, **42**, 1890–1898.
6 D. Gonzalez-Rodriguez and G. Bottari, *J. Porphyrins Phthalocyanines*, 2009, **13**, 624–636.
7 L. Flamigni and D. Gryko, *Chem. Soc. Rev.*, 2009, **38**, 1635–1646.
8 F. D'Souza, P.-M. Smith, M. E. Zandler, A. L. McCarty, M. Itou, Y. Araki and O. Ito, *J. Am. Chem. Soc.*, 2004, **126**, 7898–7907.
9 L. Giribabu, P. S. Reeta, R. K. Kanaparthi, M. Srikanth and Y. Soujanya, *J. Phys. Chem. A*, 2013, **117**, 2944–2951.
10 O. Ito and F. D'Souza, *Molecules*, 2012, **17**, 5816–5835.
11 A. F. Mironov, Synthesis, Properties and Potential Applications of Porphyrins–Fullerenes, *Macroheterocycles*, 2011, **4**, 186–208.
12 L. Giribabu, C. V. Kumar and P. Y. Reddy, *Chem. – Asian J.*, 2007, **2**, 1574–1580.
13 K. M. Smith and M. G. H. Vicente, in *Science of Synthesis*, ed. S. M. Weinreb, Georg Thieme Verlag, Stuttgart, New York, 2004, pp. 1081–1235.
14 K. M. Smith and M. G. H. Vicente, in *Science of Synthesis*, ed. S. M. Weinreb, Georg Thieme Verlag, Stuttgart, New York, 2004, pp. 1081–1235.
15 S. G. DiMagno, V. S. Y. Lin and M. J. Therien, *J. Org. Chem.*, 1993, **58**, 5983.
16 J. Kandhadi, R. K. Kanaparthi and L. Giribabu, *J. Porphyrins Phthalocyanines*, 2012, **16**, 282–289.
17 A. de la Escosura, M. V. Martinez-Diaz, P. Thordarson, A. E. Rowan, R. J. M. Nolte and T. Torres, *J. Am. Chem. Soc.*, 2003, **125**, 12300–12308.
18 A. Medina, C. G. Claessens, G. M. A. Rahman, A. M. Lamsabhi, O. Mó, M. Yanez, D. M. Guldi and T. Torres, *Chem. Commun.*, 2008, 1759–1761.
19 J. Ch. Lee, T. Y. Kim, S. H. Kang and Y. K. Shim, *Bull. Korean Chem. Soc.*, 2001, **22**, 257.
20 H. Jia, B. Schmid, S. H. Liu, M. Jaggi, P. Monobaron, S. V. Bhosale, S. Rivadehi, S. J. Langford, L. Sanguinet, E. Levillain, M. E. El-Khouly, Y. Morita, S. Fukuzumi and S. Decurtins, *ChemPhysChem*, 2012, **13**, 3370–3382.
21 S. Rai and M. Ravikanth, *Chem. Phys. Lett.*, 2008, **453**, 250–255.
22 M. Stepien, B. Donnio and J. L. Sessler, *Angew. Chem., Int. Ed.*, 2007, **119**, 1453–1457.
23 A. Osuka, E. Tsurumaki and T. Tanaka, *Bull. Chem. Soc. Jpn.*, 2011, **84**, 679–697.
24 H. Maeda and H. A. Furuta, *Pure Appl. Chem.*, 2006, **78**, 29–44.
25 B. C. Popere, A. M. D. Pelle and S. Thayumanavan, *Macromolecules*, 2011, **44**, 4767–4776.
26 M. Tasior, D. T. Gryko, J. Shen, K. M. Kadish, T. Becherer, H. Langhals, B. Ventura and L. Flamigni, *J. Phys. Chem. C*, 2008, **112**, 19699–19709.
27 C. M. Lemon and P. J. Brothers, *J. Porphyrins Phthalocyanines*, 2011, **15**, 809–834.

Published on 31 luglio 2015. Downloaded by Fail Open on 23/07/2025 10:08:23.

28 K. Sudhakar, V. Velkannan and L. Giribabu, *Tetrahedron Lett.*, 2012, **53**, 991–993.
29 B. Ventura, A. DegliEsposti, B. Koszarna, D. T. Gryko and L. Flamigni, *New J. Chem.*, 2005, **29**, 1559–1566.
30 J. Bendix, I. J. Dmochowski, H. B. Gray, A. Mahammed, L. Simkhovic and Z. Gross, *Angew. Chem., Int. Ed.*, 2000, **39**, 4048–4051.
31 L. Giribabu, J. Kandhadi and R. K. Kanaparthi, *J. Fluoresc.*, 2014, **24**, 569–577.
32 L. Giribabu, J. Kandhadi, R. K. Kanaparthi and P. S. Reeta, *J. Lumin.*, 2014, **145**, 357–363.
33 G. Rotas, G. Charalambidis, L. Galtzl, D. T. Gryko, A. Kahnt, A. G. Coutsolelos and N. Tagmatarchis, *Chem. Commun.*, 2013, **49**, 9128–9130.
34 T. H. Ngo, F. Nastasi, F. Puntoriero, S. Campagna, W. Dehaen and W. Maes, *Eur. J. Org. Chem.*, 2012, 5605–5617.
35 F. D'Souza, R. Chitta, K. Ohkubo, M. Tasior, N. K. Subbaiyan, M. E. Zandler, M. K. Rogacki, D. T. Gryko and S. Fukuzumi, *J. Am. Chem. Soc.*, 2008, **130**, 14263–14272.
36 M. Tasior, D. T. Gryko, J. Shen, K. M. Kadish, T. Becherer, H. Langhals, B. Ventura and L. Flamigni, *J. Phys. Chem. C*, 2008, **112**, 19699–19709.
37 M. Tasior, D. T. Gryko, M. Cembor, J. S. Jaworski, B. Venturac and L. Flamigni, *New J. Chem.*, 2007, **31**, 247–259.
38 L. Giribabu, K. Sudhakar, R. K. Kanaparthi and G. Sabapathi, *J. Photochem. Photobiol., A*, 2014, **284**, 18–26.
39 M. E. El-Khouly, S. Y. Shaban, O. Ito and N. Jux, *J. Porphyrins Phthalocyanines*, 2007, **11**, 719–728.
40 D. Curiel, K. Ohkubo, J. R. Reimers, S. Fukuzumi and M. J. Crossley, *Phys. Chem. Chem. Phys.*, 2007, **9**, 5260–5266.
41 B. Koszarna and D. T. Gryko, *J. Org. Chem.*, 2006, **71**, 3707–3717.
42 L. Zhang, S. Zeng, L. Yin, C. Ji, K. Li and Y. Li, *New J. Chem.*, 2013, **37**, 632–639.
43 L. Giribabu, C. V. Kumar, V. G. Reddy, P. Y. Reddy, Ch. S. Rao, S. R. Jang, J. H. Yum, M. K. Nazeeruddin and M. Gratzel, *Sol. Energy Mater. Sol. Cells*, 2007, **91**, 1611–1617.
44 M. J. Frisch, G. W. Trucks, H. B. Schlegel, G. E. Scuseria, M. A. Robb, J. R. Cheeseman, G. Scalmani, V. Barone, B. Mennucci and G. A. Petersson, *Gaussian 09 Revision A.01*, Gaussian, Inc., Wallingford CT, 2009.
45 P. H. Kumar, Y. Venkatesh, D. Siva, B. Ramakrishna and P. R. Bangal, *J. Phys. Chem. A*, 2015, **119**, 1267–1278.
46 W. W. Wadsworth and W. D. Emmons, *J. Am. Chem. Soc.*, 1961, **83**, 1733–1738.
47 D. T. Gryko, J. Piechowska, J. S. Jaworski, M. Galezowski, M. Taisor, M. Cembor and H. Butenschon, *New J. Chem.*, 2007, **31**, 1613–1619.
48 J. Bendix, I. J. Domochowski, H. B. Gray, A. Mahammed, L. Simkhovich and Z. Gross, *Angew. Chem., Int. Ed.*, 2000, **39**, 4048–4051.
49 M. Mastronian, W. Zhu, M. Stefenalli, S. Nardis, F. R. Fronczek, K. M. Smith, Z. Ou, K. M. Kadish and R. Paolesse, *Inorg. Chem.*, 2008, **47**, 11680–11687.
50 J. S. Baskin, H. Z. Yu and A. H. Zewail, *J. Phys. Chem. A*, 2002, **106**, 9837–9844.
51 H. Z. Yu, J. S. Baskin and A. H. Zewail, *J. Phys. Chem. A*, 2002, **106**, 9845–9854.
52 R. A. Marcus and N. Sutin, *Biochim. Biophys. Acta*, 1985, **811**, 265–322.
53 N. Banerji, S. V. Bhosale, I. Petkova, S. J. Langford and E. Vauthey, *Phys. Chem. Chem. Phys.*, 2011, **13**, 1019–1029, and references therein.
54 P. T. Anusha, D. Swain, S. Hamad, L. Giribabu, T. S. Prashant, S. P. Tewari and S. V. Rao, *J. Phys. Chem. C*, 2012, **116**, 17828–17837.
55 L. Zhang, Z. Y. Liu, X. Zhang, L.-L. Wang, H. Wang and H.-Y. Liu, *Photochem. Photobiol. Sci.*, 2015, **14**, 953–962.
56 S. K. Suguna, B. Robotham, R. P. Sloan, J. Szmytkowski, K. P. Ghiggino, M. F. Paige and R. P. Steer, *J. Phys. Chem. A*, 2011, **115**, 12217–12227.
57 A. Morandeira, L. Engeli and E. Vauthey, *J. Phys. Chem. A*, 2002, **106**, 4833–4837.
58 I. H. M. van Stokkum, D. S. Larsen and R. van Grondelle, *Biochim. Biophys. Acta*, 2004, **1657**, 82–104.
59 J. J Snellenburg, S. P Laptenok, R. Seger, K. M. Mullen and I. H. M. van Stokkum, *J. Stat. Soft.*, 2012, **49**, 1–22.
60 S. Prashanthi, P. H. Kumar, L. Wang, A. K. Perepogu and P. R. Bangal, *J. Fluoresc.*, 2010, **20**, 571–580.
61 M. L. Horng, J. A. Gardecki, A. Papazyan and M. Maroncelli, *J. Phys. Chem.*, 1995, **99**, 17311–17337.
62 I. Rips and J. Jortner, *J. Chem. Phys.*, 1988, **88**, 818.

 This journal is © the Owner Societies 2015